Autonomous colloidal crystallization in a galvanic microreactor

Christian Punckt, Linda Jan, Peng Jiang,[a] Thomas A. Frewen,[b] Dudley A. Saville, Ioannis G. Kevrekidis, and Ilhan A. Aksay[c]
Department of Chemical and Biological Engineering, Princeton University, Princeton, New Jersey 08544, USA

(Received 12 June 2012; accepted 30 August 2012; published online 3 October 2012)

We report on a technique that utilizes an array of galvanic microreactors to guide the assembly of two-dimensional colloidal crystals with spatial and orientational order. Our system is comprised of an array of copper and gold electrodes in a coplanar arrangement, immersed in a dilute hydrochloric acid solution in which colloidal micro-spheres of polystyrene and silica are suspended. Under optimized conditions, two-dimensional colloidal crystals form at the anodic copper with patterns and crystal orientation governed by the electrode geometry. After the aggregation process, the colloidal particles are cemented to the substrate by co-deposition of reaction products. As we vary the electrode geometry, the dissolution rate of the copper electrodes is altered. This way, we control the colloidal motion as well as the degree of reaction product formation. We show that particle motion is governed by a combination of electrokinetic effects acting directly on the colloidal particles and bulk electrolyte flow generated at the copper-gold interface.
 [http://dx.doi.org/10.1063/1.4755807]

I. INTRODUCTION

The use of colloidal crystals has been demonstrated in a variety of contexts ranging from fundamental studies of phase transitions and crystalline materials[1–5] to applications in sensor devices[6–9] and photonic band gap materials.[10–14] A remaining challenge is the controlled deposition of colloids on a substrate. Various assembly techniques, such as evaporation and spin coating methods,[11,14–19] the use of external electric fields,[20–25] and surface modifications inducing entropic interactions between colloidal particles and patterned substrates[26] have been developed for this purpose.

Deposition of colloidal particles in an autonomous fashion (no external controller and energy supply) at a predefined location and with control of the aggregate structure, however, requires the utilization of built-in energy sources and guiding mechanisms. The use of spontaneously occurring electrochemical reactions within micron-size systems is a promising route towards achieving this goal. It has been demonstrated[27–29] that by using hydrogen peroxide as a fuel, electrolyte flow can be generated at interfaces between electrochemically dissimilar metals (e.g., silver and gold). This effect has been used in catalytic nanomotors and micropumps,[30–32] and a theoretical treatment of the underlying reaction kinetics attributes the observed phenomena to complex induced-charge electrokinetics.[33–36] More recently, Liu and Sen published a study on micro swimmers which are propelled as a result of metal dissolution in a galvanic microbattery.[37] In all these approaches, however, colloidal particles are either self-propelled,[28,29,37] rendering deposition at defined target sites difficult to achieve, or the systems are designed for flow generation (pumps) in which case suspended colloidal particles are used as tracers and may form patterns according to the generated flow fields,[29,30] but adherence to the substrate is not achieved.

We present a new technique for the autonomous assembly and subsequent cementation of colloidal microspheres with spatial and orientational control that produces highly ordered colloidal crystals and provides an opportunity to create complex two-dimensional patterns. We use an array of galvanic microreactors formed by copper and gold electrodes in a coplanar geometry, immersed in a dilute hydrochloric acid solution in which polystyrene (PS) microspheres are suspended. This system does not require the supply of external (electrical) energy since the driving force of colloidal aggregation is the galvanic dissolution of the sacrificial copper anodes. By changing electrode geometry, we can tune the rate of copper dissolution and, consequently, the aggregation dynamics and the cementation of the colloidal particles. Our approach is expected to be applicable for the deposition of a variety of colloidal particles at galvanic anodes and thus has the potential to be of use in corrosion protection or adaptive (self-healing) systems.

II. EXPERIMENTAL SETUP

Colloidal aggregation and crystallization experiments were conducted in a galvanic cell consisting of an array of sacrificial copper anodes embedded in a gold cathode (Fig. 1(a)). The electrode structures were prepared as follows: A 10 nm titanium film was deposited on a silicon wafer followed by deposition of a 100 nm thick gold film using e-beam evaporation (Innovative Systems Engineering, Warminster, PA). Electroless plating in a solution of 1.5 g copper sulfate, 7.0 g potassium sodium tartrate, 2.0 g sodium hydroxide, and 5 ml formaldehyde in 50 ml of de-ionized (DI) water at room temperature was used to coat the gold film with a copper layer of thicknesses up to 70 nm (adjusted by

[a]Present address: Department of Chemical Engineering, University of Florida, Gainesville, Florida 32611, USA.
[b]Present address: United Technologies Research Center, 411 Silver Lane, East Hartford, Connecticut 06118, USA.
[c]Author to whom correspondence should be addressed. Electronic mail: iaksay@princeton.edu.

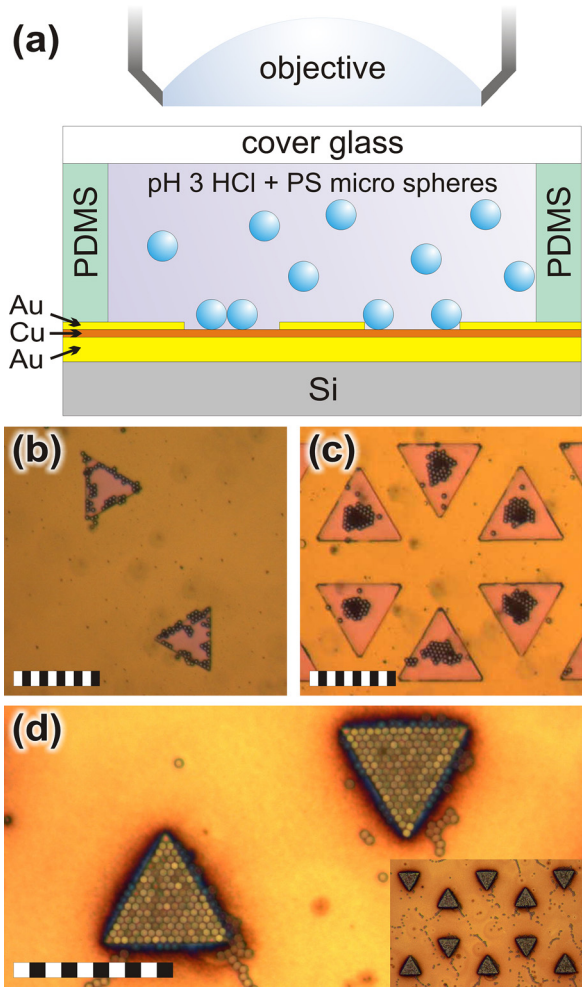

FIG. 1. Guided colloidal aggregation using galvanic microreactor arrays. (a) Schematic of the microreactor (not to scale). See text for details. (b-c) In situ images of PS particles aggregating preferentially at the edges (b) or near the centers (c) of triangular copper electrodes (enhanced online). In (c) the onset of double layer formation can be seen as dark structures covering parts of the colloidal crystals. After termination of the experiment and rinsing, however, only the first layer of colloidal particles remains cemented to the electrode. (d) 2D colloidal crystals on triangular electrodes after termination of the experiment and rinsing with DI water. Inset: larger area view. Around each particle-covered electrode, a dark halo can be seen which we attribute to the deposition of reaction products on the gold cathode (see below). Scale bars: 50 μm [URL: http://dx.doi.org/10.1063/1.4755807.1] [URL: http://dx.doi.org/10.1063/1.4755807.2].

variation of the plating time). This copper film was then photolithographically patterned with photoresist. Finally, we deposited a 200 nm gold layer on the photoresist pattern and performed a lift-off (ultrasonication in acetone) followed by washing in methanol and isopropanol. This resulted in "lowered" trench-like copper electrodes. To minimize the formation of oxide layers on the copper surfaces, samples were stored in dry nitrogen and pre-etched in *p*H 3 hydrochloric acid for 5–10 s prior to each experiment. These trenched copper electrodes were used for guided particle assembly.

Particle tracking experiments and measurements of the local copper dissolution rate were performed using raised copper electrode lines in order to avoid artifacts during the image analysis, caused by the edges of copper trenches, and to facilitate particle tracking analysis. For the fabrication of raised copper electrodes, the copper layer was etched in ~0.1 M nitric acid after patterning with photoresist, and washed in acetone, methanol, and isopropanol. No additional gold coating was applied.

Electrochemical cells were assembled by placing a polydimethylsiloxane (PDMS) ring on the patterned copper-gold electrode, filling the enclosed area with a defined amount (usually 10–30 μl) of electrolyte solution and covering the PDMS ring with a clean microscope cover glass. The electrolyte was a suspension of sulfate-PS (Invitrogen Corporation, Carlsbad, CA) or silica microspheres (Bangs Laboratories Inc., Fishers, IN) of different sizes in *p*H 3 hydrochloric acid solution. Aggregation experiments were conducted using a suspension of 0.11 vol. % PS particles, 650 μm thick PDMS spacer, and 13 min reaction time. A suspension of 0.22 vol. % PS particles and 0.16 vol. % silica particles (both ≈3 μm in diameter) in *p*H 3 HCl solution was used for particle separation experiments. For particle tracking and detailed analysis of particle motion on the copper electrodes, more dilute suspensions with concentrations down to 0.02 vol. % were used. Experiments were terminated by disassembly of the system and immediate rinsing under DI water, followed by drying under a stream of nitrogen.

The motion of the suspended colloidal particles as well as the dissolution of copper anodes were observed with an optical microscope (Zeiss Axioplan 2, Carl Zeiss Microimaging Inc., Thornwood, NY). Image sequences were recorded using a 12 bit digital CCD camera (Zeiss AxioCam HRc) and stored on a computer for further analysis. Reaction products (RPs) and aggregated particles were further analyzed *ex situ* using a scanning electron microscope (SEM, Vega 1, Tescan USA Inc., Cranberry Twp., PA).

For the analysis of the crystallinity of colloidal aggregates, image processing (contrast adjustment and thresholding) and analysis (colloidal particle centroid extraction) were performed using the open-source image processing package IMAGEJ[38] with the PointPicker plugin (Philippe Thévenaz, Biomedical Imaging Group, Swiss Federal Institute of Technology, Lausanne, Switzerland). The experimental images were first converted to grayscale and their contrast and brightness were adjusted prior to creation of a binary sample image by thresholding. Particle analysis on the binary image identified the centroids of colloidal particles; the PointPicker plugin allowed for manual user adjustment of particle centroid locations. The latter feature was useful for the small number of instances in which a single particle was incorrectly identified (e.g., the centroid of a cluster of particles was instead detected).

III. RESULTS

Once the copper and gold electrodes are exposed to the acidic particle suspension, the copper electrodes dissolve:[39] metallic copper is oxidized forming soluble copper chloride complexes ($CuCl_2^-$, likely through a Cu^+ intermediary) and cupric ions (Cu^{2+}).[40–42] This process is balanced by the reduction of dissolved oxygen on the gold cathodes (dissolution of the copper electrodes in a de-aerated electrolyte is insignificant on the time scale of our experiments), consuming

hydronium ions (H_3O^+) to produce hydrogen peroxide (H_2O_2).[43] H_2O_2, subsequently, is either electrochemically reduced at the gold cathode to form water or, if it diffuses towards copper metal, is consumed during copper oxidation.[42] The charge transfer due to Faradaic reactions on the electrode/electrolyte interfaces gives rise to an ionic current flowing through the electrolyte which is balanced by a flux of electrons through the metal electrodes from the copper to the gold.

As copper dissolution proceeds, we observe with *in situ* optical microscopy that PS particles travel towards the nearest copper anodes (Figs. 1(b) and 1(c), videos 1(b) and 1(c)) over distances up to several hundred μm. There, they form crystalline aggregates and later become immobilized and adherent to the substrate, such that after termination of the experiment, they are not removed during electrode rinsing and drying (Fig. 1(d)).

Surprisingly, we find that the location of initial particle aggregation varies as a function of the geometry of the electrode array: in the case of large spacing between the copper electrodes, particle aggregation initiates at the electrode edges (Fig. 1(b)), and particles form crystals that are aligned with the edge. At small electrode separation, however, particles first aggregate randomly at the inner region of the copper electrodes (Fig. 1(c)), subsequently forming polycrystalline patches with no pre-defined orientation. We utilize this effect to control microstructure and orientation of the crystals: geometries where edge-aggregation is observed cause particle alignment, resulting in a single-crystalline particle layer covering the electrodes (Fig. 1(d)). Conversely, with electrode geometries resulting in interior aggregation of the microspheres, we only observe the formation of polycrystals. The microstructure of deposits also depends on the nature of the electrode edge. With copper electrodes that are elevated with respect to the gold, no single crystalline colloid layer can be obtained. Only copper trench electrodes which are lowered with respect to the gold surface (see Fig. 1(a)) result in a well-aligned line of particles along the electrode edge due to the presence of a physical barrier. The alignment with respect to physical barriers and its positive impact on crystallinity is a well known effect and was studied previously for the evaporation of latex particle suspensions in micro channels[44] and electro-phoretic deposition of latex particles in photoresist-patterned electrodes.[45]

Figure 2(a) shows an SEM image of cemented PS particles on the substrate. A layer of deposited particles with approximately cubic shape (indicating crystalline nature) and about 200 nm in size can be seen underneath the colloidal particles, completely covering the surface of the substrate. Electron backscattered diffraction (EBSD) indicates that these particles consist of crystalline copper hydroxide and copper oxide species (most likely cuprous oxide, Cu_2O) which must have been generated as a result of the dissolution of the copper electrode.

For a given concentration of colloidal particles in suspension, the amount of RPs, detectable at the former location of the copper electrodes after dissolution has stopped, is correlated with the electrode geometry: we observe that a geometry corresponding to large copper surface coverage

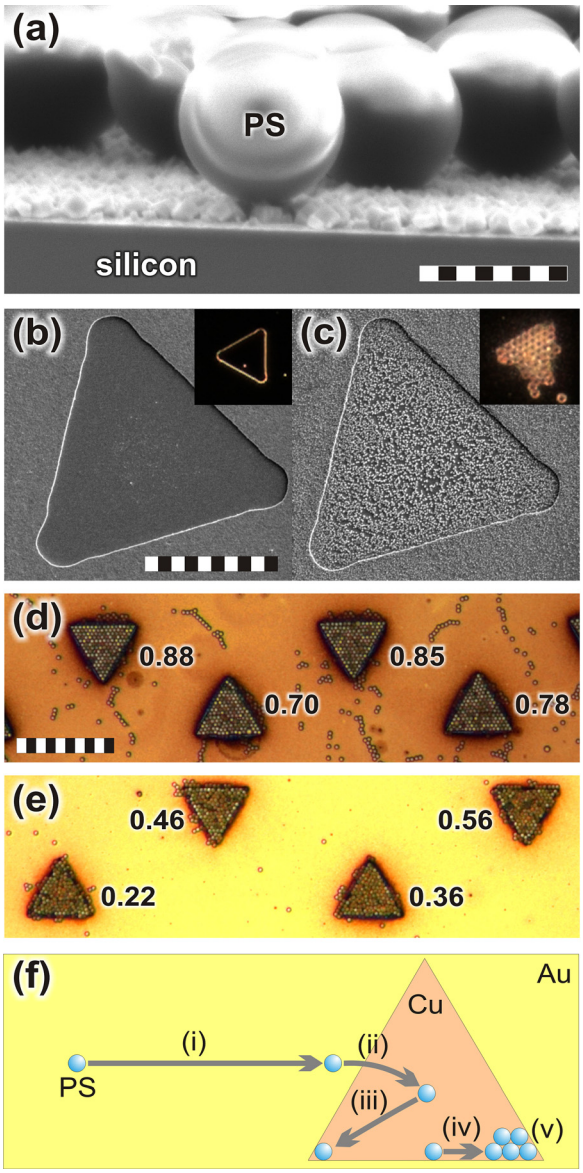

FIG. 2. Particle cementation and crystallinity of aggregates. (a) PS particles aggregated on top of a reaction product layer. Scale bar 2 μm. (b-c) SEM images of a 20 μm triangle from an array of triangles with (b) 80 μm and (c) 40 μm separation used in an aggregation experiment after sonication. Scale bar 10 μm. Insets: Optical dark-field images before sonication. (d) Section of the result presented in Fig. 1(d) (40 μm triangles with a separation of 60 μm), (e) colloidal particles aggregated on 40 μm triangles with a separation of 80 μm (experiment conducted at reduced particle volume fraction of 0.06%). Values of the calculated order parameter ψ_6 are displayed next to the respective triangular electrodes. (f) Schematic showing different stages of the particle aggregation process (see text).

(e.g., small electrode spacing) results in more RP deposition than a geometry where the surface area of the copper electrode with respect to the gold is small. This is shown in Figures 2(b) and 2(c) where we compare the RP coverage of 20 μm copper triangles at an electrode spacing of 80 μm (no RPs visible) and a spacing of 40 μm (RPs are present). Layers of colloidal particles which are deployed onto these electrodes and form colloidal crystals rinse off easily in the absence of RPs (inset of Fig. 2(b)) but stick if RPs are present (inset of Fig. 2(c)). Thus, copper oxide and hydroxide layers forming during the dissolution process probably serve as "glue" that binds colloidal particles to the electrode

surface, such that only ultrasonication can remove them from the surface.

In order to obtain single crystalline colloidal aggregates, however, particles need to remain mobile on the copper electrode for a sufficient amount of time before cementation occurs, such that "Brownian annealing" arranges them properly relative to the particles already aligned with the electrode edges. This is achieved if the electrode spacing is within an optimum range as shown in Figures 2(d) and 2(e). A comparison of the results obtained with $s = 60\,\mu m$ (also shown above in Figure 1(d)) and $s = 80\,\mu m$ reveals that for $s = 60\,\mu m$ the PS particles remained Brownian on the Cu electrode for a sufficiently long time in order to form a single-crystal structure before cementation occurred, while at larger electrode spacing the particles are Brownian only for a short time (a few seconds at most) such that they do not form a high-quality colloidal crystal.

We quantified the crystallinity of aggregated colloidal particles and studied the impact of parameter changes on the aggregation process quantitatively by calculating, for a given experimental setting, an order parameter for each colloidal particle-covered copper electrode.[46,47] As a measure for the order of colloidal aggregates, we use a bond orientational order parameter which is well established as a generic measure of crystallinity.[46,47] For each colloidal particle in the sample, we identify its nearest neighbors via the construction of Voronoi polyhedra.[48] The local orientational order parameter ψ_6 for a particle k is given by[47]

$$\psi_6^k = \frac{1}{N_k}\sum_l \exp(6i\theta_{kl}), \tag{1}$$

where the sum is calculated over the N_k neighboring particles. θ_{kl} denotes the angle between the particle-particle bond and a fixed reference axis. A global order parameter is computed by averaging ψ_6 over all particles in a sample and calculating the modulus

$$\psi_6 = \left|\frac{1}{N}\sum_k \psi_6^k\right|. \tag{2}$$

Quantitative data obtained with this approach are shown in Figures 2(d) and 2(e) and emphasize the strong dependence of the result of the aggregation process on a careful tuning of the reaction parameters: The average ψ_6 values for $s = 60\,\mu m$ (Fig. 2(d)) and $s = 80\,\mu m$ (Fig. 2(e)) are 0.78 ± 0.10 and 0.34 ± 0.17, respectively (each including data from more than 10 electrodes). Thus, with insufficient Brownian annealing at $s = 80\,\mu m$, we obtain a significantly lower degree of order in the colloidal aggregate than with prolonged Brownian annealing. Factors controlling the duration of Brownian annealing are likely complex in nature and involve the balance between reaction rate, diffusive transport of ionic species, RP precipitation, and attractive electrokinetic forces "pulling" the PS particles towards the electrode surface.

Closer examination of the trajectories of individual particles during the aggregation process reveals that the aggregation process can be divided into five distinct stages (Fig. 2(f)): (i) Particles suspended in the electrolyte move towards the copper anodes over distances up to several hundred microns (long-range transport). (ii) As PS particles approach the copper anodes, they are pulled down to the copper surface, resulting in the particles being located immediately on top of the copper electrodes (short-range attraction). (iii) Individual particles on the surface of the copper electrode exhibit Brownian motion and may move towards the electrode edges or corners. (iv) Particles which remain mobile on the copper electrode exhibit attractive interaction and eventually form crystalline patches. These patches often remain visibly mobile and move towards other particle aggregates or electrode edges. (v) Eventually, colloidal particles can become immobilized and stick to the electrode surface, such that they cannot be removed from the substrate by rinsing after termination of the experiment.

In order to probe long-range particle motion (stage (i)) both in the bulk electrolyte and near the substrate, we conducted additional experiments using $50\,\mu m$ wide copper line electrodes spaced $160\,\mu m$ apart and a mixture of neutrally buoyant dyed PS and denser silica particles (sedimentation velocity $\approx 5\,\mu m/s$) which settle down during the experiment (Figs. 3(a) and 3(b)). We find that within the bulk electrolyte, in a plane $y \approx 20\,\mu m$ above the cathodic gold surface both PS and silica particles are transported towards the nearest copper electrode with velocities between 1 and $2\,\mu m/s$. For silica particles, this lateral motion comes to a halt and then gradually reverses while they approach the surface of the gold cathode during sedimentation (Fig. 3(b), see also schematic in Fig. 4(a)). On the cathode ($y = 0\,\mu m$), silica particles move laterally away from the nearest copper electrode with velocities of more than $1\,\mu m/s$ (Fig. 3(b)). As a result, PS particles are exclusively depositing on the copper anode, while silica particles are mainly found on the gold cathode, where they remain as isolated Brownian particles (Fig. 3(a)).

In the following discussion, we try to shed light on the origin of these observations. We will focus on the explanation of long-range transport of colloidal particles (stage (i)), briefly address short-range attraction (stage (ii)), preferential aggregation (stage (iii)) and particle crystallization (stage (iv)), and finally discuss effects leading to particle cementation (stage (v)).

IV. DISCUSSION

If particle motion during long-range particle transport was solely due to effects such as electrophoresis (EP), dielectrophoresis (DEP), or diffusiophoresis (DP), the direction of the motion should be solely determined by the direction of the electric field and its gradient, the particle charge, and the concentration profile of ions in the electrolyte. Nonetheless, we observe a sign change in the velocity of silica particles (Fig. 3(b)) as they approach the gold cathode. This observation led us to conclude that bulk fluid flow must be the origin of long-range particle motion.

Using an order-of-magnitude estimate of the electric fields, we can demonstrate that transport of particles over lateral distances of several hundred micrometers as observed cannot be attributed to EP, and that EP only affects particle motion in close vicinity of the electrodes: our dielectric

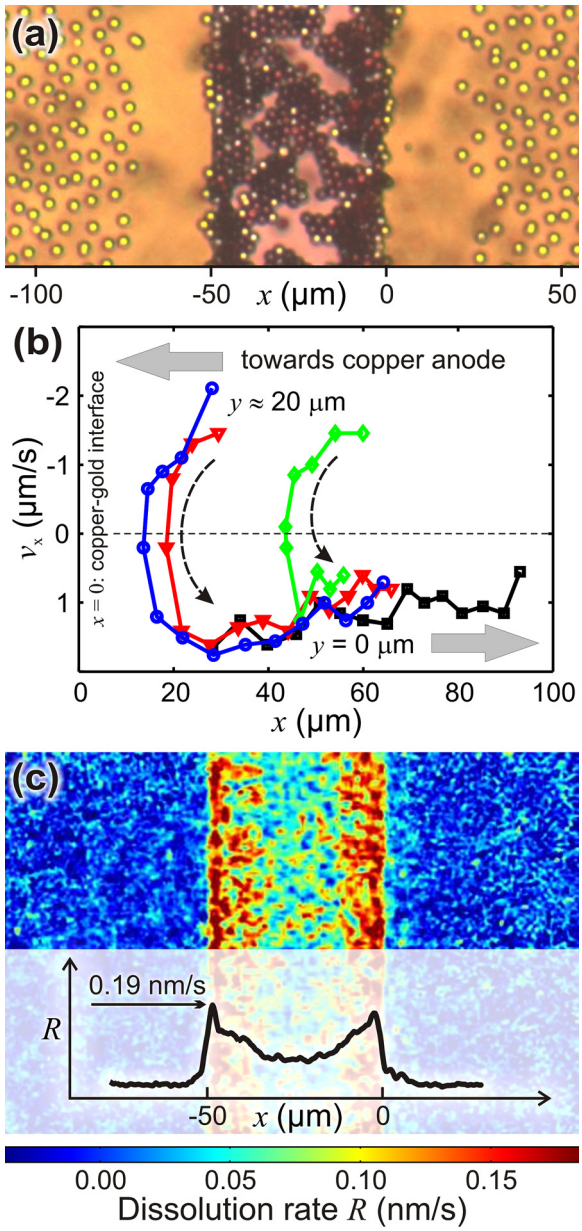

FIG. 3. (a) Separation of PS (dark) and silica (bright) particles during dissolution of a copper line electrode on gold. The x-axis indicates positions relative to right edge of copper electrode. (b) Velocity of silica particles: negative velocities correspond to a motion towards the copper anode while positive velocities indicate motion away from the copper. The x-axis corresponds to the axis shown in (a). (c) Spatially resolved dissolution rate of a 50 μm wide copper anode (for 950 μm electrode spacing).

microspheres have a radius r which is large compared to the Debye length λ_D ($r/\lambda_D > 100$) such that we can use Smoluchowski's equation to estimate the electric field E necessary to sustain a given electrophoretic velocity u_{EP}:[49]

$$u_{EP} = \frac{\varepsilon \zeta_p E}{\mu}. \tag{3}$$

Here, ε is the dielectric constant of the medium, ζ_p is the measured zeta-potential of the particle (PS: -44 mV, silica: -39 mV), and μ is the dynamic viscosity of the medium (water). From the measured velocity $v_x \approx -1.5$ μm/s of PS particles above the gold cathode ($y \approx 20$ μm) and using

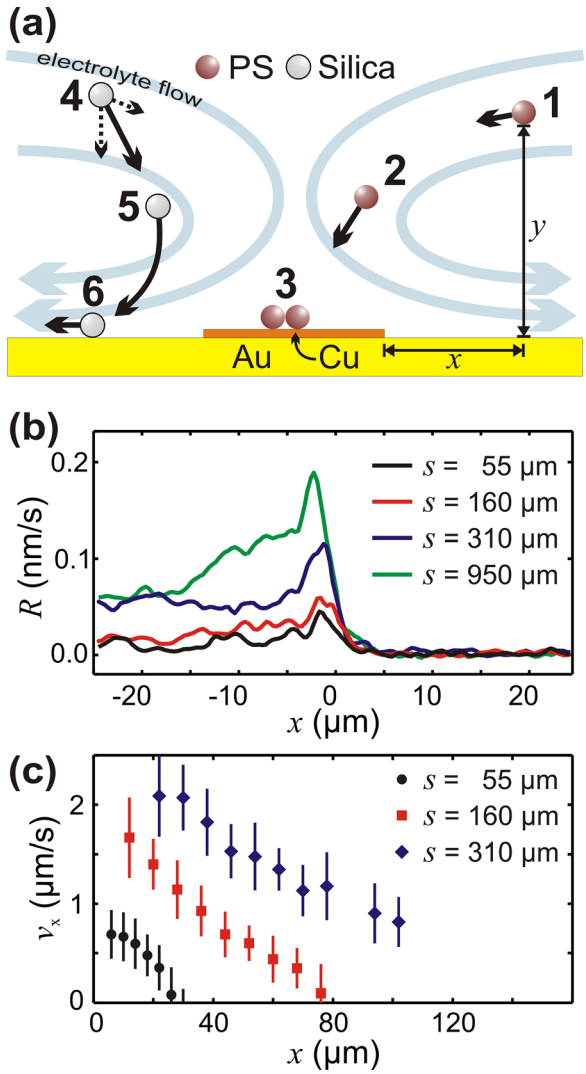

FIG. 4. (a) Schematic of bulk electrolyte flow. (b) Cross sections of dissolution rate at different electrode spacing s. (c) Velocity of silica particles located on the gold cathode ($y = 0$ μm) for different electrode spacing s.

Eq. (3), we obtain a value of $E \approx 0.5$ V/cm which would be necessary to cause particle motion through EP. We compare this estimate to the potential drop that is caused by the electrochemical reaction: With an optical technique that relies on color changes of the copper thin film during galvanic dissolution,[39] we are able to monitor the dissolution rate R of copper with spatial resolution (Fig. 3(c)). Assuming a one-electron charge transfer reaction (equivalent to $Cu \leftrightarrow Cu^+ + e^-$, but also including copper chloride complex formation), the measured maximum dissolution rate $R = 0.19$ nm/s at the edge of the copper line corresponds to a current density of about 250 μA/cm^2 which, at the given electrolyte conductivity of 400 μS/cm, results in a local electrical field of $E_x \approx 0.65$ V/cm. In this estimate, we neglect self-corrosion of the copper electrode (galvanic corrosion between adjacent copper grains) since the electrochemical overpotential generated by the cathodic gold surface is dominant.[50]

We conclude that only in the direct vicinity of the dissolving copper electrodes, the electric field is sufficiently large to cause directed particle motion and likely accounts

for the PS spheres being pulled down to the substrate as they approach the electrodes (stage (ii) of particle motion). In a distance of tens or even hundreds of microns away from the copper anode, however, the electric field is too weak to cause particle motion at the observed velocities.

Similar estimates have been performed for dielectrophoretic and diffusiophoretic particle motion: The velocity u_{DEP} of dielectrophoretically induced particle motion can be calculated by balancing the dielectrophoretic force with Stokes drag, resulting in:[51]

$$u_{DEP} = \frac{\varepsilon r^2}{3\mu}\alpha \cdot \nabla |E|^2. \quad (4)$$

Here, r is the particle radius, and α is the real part of the Clausius-Mossotti factor indicating the dielectric constant contrast between particles and medium (taken to be -0.5 in case of particles with small dielectric constant in a high dielectric constant medium). For an order of magnitude estimate, we assume a current density in the electrolyte of $1\,mA/cm^2$, resulting in an electric field of $10\,V/cm$ at $100\,\mu S/cm$ conductivity and a gradient of the electric field of $10^4\,V/cm^2$ (0 to $10\,V/cm$ over $10\,\mu m$) and obtain an upper limit of $u_{DEP} = 50\,nm/s$ for PS particles even in close vicinity of the copper-gold interface.

In the case of DP, for a binary electrolyte and negligible Debye layer thickness, the particle velocity can be approximated with the following equation:[52,53]

$$u_{DP} \approx \frac{\varepsilon}{z\mu}\frac{kT}{e}\left[\beta\zeta_p - \frac{2kT}{ze}\ln(1-\gamma^2)\right]\nabla \ln C \quad (5)$$

with $\beta = \frac{D_+ - D_-}{D_+ + D_-}$ and $\gamma = \tanh\left(\frac{z\zeta_p e}{4kT}\right)$. Here, C denotes the electrolyte concentration, D_+ and D_- are the diffusion coefficients of cations and anions, and kT/e is the thermal voltage. Since we lack the detailed knowledge of the chemistry of our system necessary for assessing the contribution of each ionic species individually, we restrict ourselves to an order of magnitude estimate of an upper limit for DP-induced particle motion based on the HCl background electrolyte. For our calculation, we assume that the formation of copper chloride complexes consumes chloride ions according to $Cu + 2Cl^- \leftrightarrow CuCl^{2-} + e^-$,[42] and we further assume that the complexes remain stable over time and do not undergo subsequent reactions. This second assumption results in an overestimation of the decrease in chloride ion concentration C_{Cl-} since subsequent reactions, such as the precipitation of cuprous oxide, release chloride ions as a reaction product[42] and thus counteract the local decrease in C_{Cl-}.

Using Comsol®, we performed a simple calculation of the distribution of C_{Cl-} in an array of $50\,\mu m$ wide copper lines separated by $250\,\mu m$ wide gold cathodes based on the time-dependent solution of Fick's diffusion law. C_{Cl-} in the bulk was initially set to 1 mM, anodes were assigned an outward flux of magnitude $20\,\mu Ms^{-1}\,m^{-2}$ (corresponding to an average dissolution rate of 0.1 nm/s, as typically observed in our experiments), and all other boundaries were set to no flux. As a result, we obtained profiles of C_{Cl-} and ∇C_{Cl-} near the electrode surface. At a lateral distance of $50\,\mu m$ away from the copper-gold interface, we obtained $C_{Cl-} \approx 0.8\,mM$ and $\nabla C_{Cl-} \approx 1.7\,M/m$ at a time $t = 10\,s$. Using Eq. (5) and diffusion coefficients of $9.31 \times 10^{-5}\,cm^2/s$ and $2.03 \times 10^{-5}\,cm^2/s$ for hydronium and chloride ions, respectively, we calculated an upper limit of the diffusiophoretic particle velocity of $u_{DP} \approx -0.7\,\mu m/s$ both for PS and silica particles whose motion consequently is directed toward decreasing C_{Cl-}.

This value is only slightly smaller than the observed velocities of silica particles in the bulk electrolyte shown in Figure 3(b) ($y = 20\,\mu m$), but it needs to be emphasized that it is the result of overestimating the decrease in C_{Cl-}. More importantly, however, silica particles on the gold cathode ($y = 0\,\mu m$) should experience a similar diffusiophoretic attraction towards regions of low C_{Cl-} as particles suspended in the bulk electrolyte. Instead, we observe silica particles on the gold electrode moving away from the copper-gold interfaces (Fig. 3(b)) although concentration changes originate from these high dissolution rate locations. We conclude that DP has negligible impact on long-range particle motion and only plays a role in the direct vicinity of electrode edges where concentration gradients are at their maximum. For a complete assessment of the role of DP, however, a detailed theoretical study of the electrochemical and electrokinetic phenomena in our system is necessary.

We suggest that, instead of electrokinetic effects acting directly on the suspended colloidal particles, bulk fluid flow is predominantly responsible for long-range particle transport, as schematically illustrated in Figure 4(a). This diagram shows the simplest flow pattern that would be consistent with our experimental results. PS and silica particles in the bulk of the electrolyte (i.e., at a distance $y > 20\,\mu m$ above the gold surface) are transported towards the nearest copper electrode by bulk electrolyte flow (positions 1 and 4 in Figure 4(a)). While light PS particles are entrained in the flow, silica particles sink down to the gold surface (positions 5 and 6) where a reverse flow away from the copper electrode dominates their motion. Thus, as they sink down to the gold surface, the motion of silica particles reverses and they are transported away from the copper electrodes (compare Figure 3(b)). Only silica particles which are located right above a copper electrode (or in sufficiently close vicinity to not become entrained in the reverse flow) can deposit on copper. The PS particles, on the other hand, are transported into the direct vicinity of the copper electrodes (position 2 in Figure 4(a)) where they most likely become attracted to the copper through electrophoresis.

We find a positive correlation between the spacing s of copper electrodes and the dissolution rate R (Fig. 4(b)). This can most likely be explained by the larger available cathodic surface area for oxygen reduction (which is limiting the overall reaction rate kinetically[50]) and by the increased diffusive transport of RPs and educts at the anode (reducing dissolution rate-decreasing effects of concentration overpotential) when s is large.[39] The increased electrochemical reaction rate due to increased electrode spacing is correlated with an increased velocity of silica particles moving away from the copper-gold interface as they have reached the gold

surface (Fig. 4(c)). This suggests that the rate of the electrochemical reaction determines the strength of electrolyte flow and thus the velocity of suspended colloidal particles. Furthermore, R is spatially heterogeneous: For the largest electrode spacing of $s = 950\ \mu$m, we observe $R = 0.06$ nm/s in the electrode center, and values up to $R = 0.19$ nm/s at the copper-gold interface. Since the electrolyte flow is certainly of electrokinetic origin, we contend that the flow is generated mostly within a small region near the copper-gold interface where the magnitude of Faradaic currents and, correspondingly, the strength of the electric field is at their maximum.

Our observation that fluid flow scales with dissolution rate and electrode spacing (cathode size) shown in Figures 4(b) and 4(c) is in agreement with the most recent theoretical studies of electrochemically induced flows in binary[35] and multicomponent[33,36] electrolytes. The authors of these studies attributed electrolyte flow to so-called reaction-induced charge auto-electrophoresis:[33,36] on a surface passing a Faradaic current, an "electro-osmotic" slip flow emerges as a result of electric body forces which are generated through the charge- and field distribution as effected by the Faradaic reaction itself. It was found that flow velocity scales linearly with total Faradaic current and system size. Additionally, our measurement of the spatial distribution of the dissolution rate (Figs. 3(c) and 4(b)) suggests that also the degree of spatial heterogeneity of the current plays an important role in the development of bulk electrolyte flow. For binary electrolytes and small current density, Ristenpart *et al.*[54] conducted a theoretical treatment of heterogeneity-induced fluid flow and colloidal transport that could in part also explain our experimental observations of strong electrolyte flow being correlated with highly localized Faradaic currents at the electrode edges. However, our dissolving copper electrodes exhibit current densities that probably exceed the limits of this theoretical treatment and therefore results are not directly comparable.

We conclude that variations of the bulk electrolyte flow pattern and, in the direct vicinity of the copper electrodes, EP and DEP are responsible for the observed geometry-dependent differences in preferential particle aggregation at electrode edges and centers (Figs. 1(b) and 1(c)): Larger electrode spacing s results in a strongly increased copper dissolution rate R. This in turn leads to both stronger electrolyte flow and also to an increased local electrophoretic and diffusiophoretic attraction towards the electrode edges, thus preventing light PS particles to aggregate near the electrode center. For a more complete understanding of the particle motion, a thorough theoretical analysis relating geometry-dependent electrochemical kinetics to electrohydrodynamic mechanisms causing fluid flow needs to be performed. Work in this direction is currently under way.

Both randomly distributed PS particles as well as particles aggregating preferentially at the electrode edges are drawn toward one another forming crystalline aggregates (stage (iv)). This can be attributed to well-studied electroosmotic and electrohydrodynamic phenomena that were described previously by ourselves and others[21,22,55–59] and which are usually observed by applying an external source of electric current (DC or AC) to a colloid. Instead of being applied externally, in our system such currents are the result of the electrochemical reactions taking place on the galvanic electrodes.

The observation of RPs underneath deposited PS particles suggests that, in order to understand the immobilization and cementation of colloidal particles, we must analyze the system chemistry in more detail. For different electrode geometries and system volumes, we calculated the total amounts of copper, chloride ions, hydronium ions, and dissolved molecular oxygen (all of which participate in the electrochemical reactions). We find that by varying the amount of copper, we might significantly shift chemical equilibria as is illustrated in a simplified way by the following considerations.

In the experiment shown in Figure 2(c), we have observed reaction product formation. Based on electrode thickness (40 nm), size (20 μm) and spacing (40 μm) as well as the thickness of the electrolyte layer (500 μm), we estimate that per liter of electrolyte 1.5×10^{-3} mol of copper atoms are present in the system. The concentration of hydronium as well as chloride ions is 1×10^{-3} M. In a simplified picture, to balance the dissolution of 1.5×10^{-3} mol of copper, the same amount of hydronium ions should be consumed during oxygen reduction at the gold cathode. Since copper is present in excess, we can expect a strong increase in pH due to consumption of hydronium ions which may be sufficient to lead to a condensation of RPs such as cuprous oxide which has accumulated near the copper electrodes and which is soluble in acidic environments but insoluble in neutral water.

Let us next consider the case where no RPs could be detected, shown in Figure 2(b). Here, we estimate that per liter of electrolyte only 0.5×10^{-3} mol of copper atoms are present in the system. Thus, the effect on the electrolyte pH will be less pronounced and may be insufficient to lead to condensation of cuprous oxide or other reaction products. Of course, our system chemistry is more complex than assumed above. The formation of cuprous oxide from a copper chloride complex and water, for example, will increase the electrolyte acidity and thus increase RP solubility. A more complete understanding of the chemical processes leading to RP deposition and particle cementation will require a more detailed analysis of RPs as well as monitoring of the reaction conditions *in situ* which will be the scope of a future publication.

Interestingly, in experiments that are conducted with an intermediate electrode spacing (e.g., between the cases shown in Figures 2(b) and 2(c)), the density of RPs can be also affected by the concentration of colloidal particles in suspension: in the absence of suspended colloidal particles, experiments yield no visible RPs on the copper surface. This suggests that layers of colloidal particles accumulating near the electrode surface during the colloidal crystallization process create a diffusion barrier for soluble reaction products and educts, changing their concentration near the electrode surface compared to the case where colloidal particles are absent. Such concentration changes may facilitate the formation of the RP layer cementing the colloidal particles to the substrate.

We can only hypothesize about the nature of the interactions between colloidal particles, substrate and deposited

RPs. Factors contributing to cementation might include increased van-der-Waals or hydrogen bonding between RP-covered PS particles and substrate due to a larger contact area which, in a macroscopic view, corresponds to increased friction between PS particles and substrate (resistance to rinsing) due to increased surface roughness.

V. SUMMARY

We have employed galvanic microreactors for the guided assembly of colloidal particles. Polystyrene microparticles are transported over several hundred μm towards the nearest galvanically dissolving copper electrodes where they form crystalline aggregates with well-defined orientation that are cemented to the substrate through co-depositing reaction products. Particle motion near and on the galvanic electrodes is governed by electrokinetic effects whose origin is the galvanic dissolution of copper electrodes.

Long range particle transport is caused by bulk electrolyte flow which arises at the copper-gold electrode interface. By changing the geometry of the galvanic electrodes, we can tune the dissolution rate and, consequently, the aggregation dynamics in the system. Since the energy source is the electrochemical potential difference between dissimilar surface sites (copper and gold in our demonstration), the microreactor does not require the presence of "fuel" in the electrolyte as in most of the systems described in the literature, and only requires the colloidal particles to be buoyant and to exhibit a negative ζ_p. Furthermore, the motion of colloidal particles can in principle be affected by any suitable combination of galvanic electrodes with sufficiently large electrochemical potential difference to allow for the observed effects to occur at detectable magnitude. Therefore, we envision that our technique of colloidal aggregation can be utilized in a variety of environments such as metals in contact with salt solutions exhibiting localized corrosion (e.g., pitting corrosion of steel and aluminum or intergranular corrosion of various metals), where colloidal particles will preferentially aggregate at sites exhibiting anodic dissolution.

Our combination of particle tracking (i.e., fluid flow monitoring) and spatially resolved monitoring of the copper dissolution rate[39] is particularly well suited for comparison with further theoretical studies and may help to shed more light on the underlying physics of flow generation and long-range particle transport. In addition to the well-studied experimental systems employing hydrogen peroxide decomposition,[27–29] our setup provides a broadly tunable electrochemical current (which can be measured with spatial resolution) and a multi-component electrolyte which will potentially put existing theories to a more rigorous test.

ACKNOWLEDGMENTS

We thank Boris Khusid for stimulating discussions. This work was supported by the ARO/MURI under Grant No. W911NF-04-1-0170, and NASA University Research, Engineering, and Technology Institute on BioInspired Materials (BIMat) under Award No. NCC-1-02037. C.P. acknowledges financial support from the Alexander von Humboldt Foundation. I.G.K. and T.F. were partially supported by the DARPA under Grant No. HR0011-04-1-0053.

[1]K. Q. Zhang and X. Y. Liu, Nature **429**, 739–743 (2004).
[2]A. M. Alsayed, M. F. Islam, J. Zhang, P. J. Collings, and A. G. Yodh, Science **309**, 1207–1210 (2005).
[3]P. Schall, I. Cohen, D. A. Weitz, and F. Spaepen, Nature **440**, 319–323 (2006).
[4]U. Gasser, J. Phys.: Condens. Matter **21**, 203101 (2009).
[5]Y. Peng, Z. Wang, A. M. Alsayed, A. G. Yodh, and Y. Han, Phys. Rev. Lett. **104**, 205703 (2010).
[6]J. H. Holtz and S. A. Asher, Nature **389**, 829–832 (1997).
[7]M. M. Baksh, M. Jaros, and J. T. Groves, Nature **427**, 139–141 (2004).
[8]M. Ben-Moshe, V. L. Alexeev, and S. A. Asher, Anal. Chem. **78**, 5149–5157 (2006).
[9]M. M. W. Muscatello, L. E. Stunja, and S. A. Asher, Anal. Chem. **81**, 4978–4986 (2009).
[10]A. A. Zakhidov, R. H. Baughman, Z. Iqbal, C. X. Cui, I. Khayrullin, S. O. Dantas, I. Marti, and V. G. Ralchenko, Science **282**, 897–901 (1998).
[11]Y. A. Vlasov, X. Z. Bo, J. C. Sturm, and D. J. Norris, Nature **414**, 289–293 (2001).
[12]A. P. Hynninen, J. H. J. Thijssen, E. C. M. Vermolen, M. Dijkstra, and A. Van Blaaderen, Nature Mater. **6**, 202–205 (2007).
[13]S. A. Rinne, F. Garcia-Santamaria, and P. V. Braun, Nat. Photonics **2**, 52–56 (2008).
[14]J. F. Galisteo-Lopez, M. Ibisate, R. Sapienza, L. S. Froufe-Perez, A. Blanco, and C. Lopez, Adv. Mater. **23**, 30–69 (2011).
[15]P. Jiang, J. F. Bertone, K. S. Hwang, and V. L. Colvin, Chem. Mater. **11**, 2132–2140 (1999).
[16]R. G. Shimmin, A. J. DiMauro, and P. V. Braun, Langmuir **22**, 6507–6513 (2006).
[17]D. J. Harris, H. Hu, J. C. Conrad, and J. A. Lewis, Phys. Rev. Lett. **98**, 148301 (2007).
[18]P. Jiang, C. H. Sun, N. C. Linn, B. J. Ho, and S. Venkatesh, Curr. Nanosci. **3**, 296–305 (2007).
[19]K. J. Stebe, E. Lewandowski, and M. Ghosh, Science **325**, 159–160 (2009).
[20]M. Trau, S. Sankaran, D. A. Saville, and I. A. Aksay, Nature **374**, 437–439 (1995).
[21]M. Trau, D. A. Saville, and I. A. Aksay, Science **272**, 706–709 (1996).
[22]S. R. Yeh, M. Seul, and B. I. Shraiman, Nature **386**, 57–59 (1997).
[23]W. D. Ristenpart, I. A. Aksay, and D. A. Saville, Phys. Rev. Lett. **90**, 128303 (2003).
[24]R. G. Xie and X. Y. Liu, J. Am. Chem. Soc. **131**, 4976–4982 (2009).
[25]K. Q. Zhang and X. Y. Liu, J. Chem. Phys. **130**, 184901 (2009).
[26]K. H. Lin, J. C. Crocker, V. Prasad, A. Schofield, D. A. Weitz, T. C. Lubensky, and A. G. Yodh, Phys. Rev. Lett. **85**, 1770–1773 (2000).
[27]W. F. Paxton, K. C. Kistler, C. C. Olmeda, A. Sen, S. K. St Angelo, Y. Y. Cao, T. E. Mallouk, P. E. Lammert, and V. H. Crespi, J. Am. Chem. Soc. **126**, 13424–13431 (2004).
[28]T. R. Kline, W. F. Paxton, T. E. Mallouk, and A. Sen, Angew. Chem., Int. Ed. **44**, 744–746 (2005).
[29]T. R. Kline, W. F. Paxton, Y. Wang, D. Velegol, T. E. Mallouk, and A. Sen, J. Am. Chem. Soc. **127**, 17150–17151 (2005).
[30]W. F. Paxton, P. T. Baker, T. R. Kline, Y. Wang, T. E. Mallouk, and A. Sen, J. Am. Chem. Soc. **128**, 14881–14888 (2006).
[31]J. Y. Zhang and J. M. Catchmark, Microfluid. Nanofluid. **10**, 1147–1151 (2011).
[32]A. A. Solovev, S. Sanchez, Y. F. Mei, and O. G. Schmidt, Phys. Chem. Chem. Phys. **13**, 10131–10135 (2011).
[33]J. L. Moran, P. M. Wheat, and J. D. Posner, Phys. Rev. E **81**, 065302 (2010).
[34]M. Z. Bazant and T. M. Squires, Curr. Opin. Colloid Interface Sci. **15**, 203–213 (2010).
[35]E. Yariv, Proc. R. Soc. London, Ser. A **467**, 1645–1664 (2011).
[36]J. L. Moran and J. D. Posner, J. Fluid Mech. **680**, 31–66 (2011).
[37]R. Liu and A. Sen, J. Am. Chem. Soc. **133**, 20064–20067 (2011).
[38]W. S. Rasband, IMAGEJ, U. S. National Institutes of Health, Bethesda, Maryland, USA, 1997–2008, see http://rsb.info.nih.gov/ij/.
[39]C. Punckt and I. A. Aksay, J. Chem. Phys. **131**, 244710 (2009).
[40]M. Braun and K. Nobe, J. Electrochem. Soc. **126**, 1666–1671 (1979).
[41]H. P. Lee and K. Nobe, J. Electrochem. Soc. **133**, 2035–2043 (1986).
[42]G. Kear, B. D. Barker, and F. C. Walsh, Corros. Sci. **46**, 109–135 (2004).
[43]M. A. Genshaw, A. Damjanov, and J. O. Bockris, J. Electroanal. Chem. **15**, 163–172 (1967).

[44]E. Kim, Y. N. Xia, and G. M. Whitesides, Adv. Mater. **8**, 245 (1996).
[45]E. Kumacheva, R. K. Golding, M. Allard, and E. H. Sargent, Adv. Mater. **14**, 221–224 (2002).
[46]D. R. Nelson and B. I. Halperin, Phys. Rev. B **19**, 2457–2484 (1979).
[47]A. Jaster, Europhys. Lett. **42**, 277–281 (1998).
[48]R. Collins, *Phase Transitions and Critical Phenomena* (Academic, New York, 1972), Vol. 2.
[49]W. B. Russel, D. A. Saville, and W. R. Showalter, *Colloidal Dispersions* (Cambridge University Press, Cambridge, 1989).
[50]C. M. Murira, C. Punckt, H. C. Schniepp, B. Khusid, and I. A. Aksay, Langmuir **24**, 14269–14275 (2008).
[51]H. A. Pohl, *Dielectrophoresis: The Behavior of Neutral Matter in Nonuniform Electric Fields* (Cambridge University Press, New York, 1978).
[52]B. V. Deryagin, S. S. Dukhin, and A. A. Korotkova, Kolloidn. Zh. **23**, 53 (1961).
[53]D. C. Prieve, J. L. Anderson, J. P. Ebel, and M. E. Lowell, J. Fluid Mech. **148**, 247–269 (1984).
[54]W. D. Ristenpart, P. Jiang, M. A. Slowik, C. Punckt, D. A. Saville, and I. A. Aksay, Langmuir **24**, 12172–12180 (2008).
[55]P. Richetti, J. Prost, and P. Barois, Phys. Lett. **45**, 1137–1143 (1984).
[56]M. Giersig and P. Mulvaney, J. Phys. Chem. **97**, 6334–6336 (1993).
[57]M. Böhmer, Langmuir **12**, 5747–5750 (1996).
[58]Y. Solomentsev, S. A. Guelcher, M. Bevan, and J. L. Anderson, Langmuir **16**, 9208–9216 (2000).
[59]W. D. Ristenpart, I. A. Aksay, and D. A. Saville, Langmuir **23**, 4071–4080 (2007).